Pulsar-wind nebulae and magnetar outflows: observations at radio, X-ray, and gamma-ray wavelengths

George G. Pavlov · **Oleg Kargaltsev** · **Noel Klingler**

Abstract Observations of older PWNe outside SNRs are discussed.

1 X-ray pulsar wind nebulae outside supernova remnants

1.1 Expected general properties of PWNe of supersonically moving pulsars

For the first 500–1000 years after the SN explosion, the SNR's radius $R_{\rm snr}$ almost linearly increases with time with a typical speed of $\sim 10,000$ km s^{-1}, much faster than the typical puslar speed of a few hundred km s^{-1}. At larger ages the SNR expansion slows down ($R_{\rm snr} \propto t^{2/5}$ and $t^{3/10}$ in the Sedov and pressure-driven snowplow stages, respectively), while the pulsar keeps moving with about the same velocity and eventually leaves the SNR at an age of ~ 20–200 kyr (see Fig. 4 in Arzoumanian et al. 2002). This means that most of the known pulsars are moving in the ISM with the speed $V_{\rm psr}$ considerably exceeding the speed of sound in the ambient medium, $c_s = (\gamma_{\rm ad} kT/\mu m_{\rm H})^{1/2} \sim 3$–30 km s^{-1}, where $\gamma_{\rm ad}$ is the adiabatic index ($\gamma_{\rm ad} = 5/3$ for monoatomic gases), T is the temperature, and μ is the molecular weight. The supersonic motion of the pulsar drastically changes the PWN morphology (see van der Swaluw et al. 2004, Gaensler and Slane 2006, and references therein). Since the ram pressure $p_{\rm ram} = \rho_{\rm amb} V_{\rm psr}^2 = 1.5 \times 10^{-9} n_b (V_{\rm psr}/300\,{\rm km\,s}^{-1})^2$ dyn cm^{-2} (where n_b is the ambient baryon number density in units of cm^{-3}) exceeds the ambient pressure $p_{\rm amb}$,

$$p_{\rm ram}/p_{\rm amb} = \gamma_{\rm ad} \mathscr{M}^2 \gg 1\,, \tag{1}$$

($\mathscr{M} = V_{\rm psr}/c_s$ is the Mach number), the PWN acquires a cometary shape with a compact head around the pulsar and a long tail behind it (Figure 1.1). In an idealized picture, the interaction of the pulsar wind (PW) with the ambient (circumpulsar) medium creates three distinct regions. The bullet-shaped cavity around the pulsar is filled with the *unshocked relativistic PW* confined within the termination shock (TS). The *shocked PW*, which is the main source of synchrotron radiation in X-rays, is flowing away between the TS and the contact

George Pavlov
Department of Astronomy and Astrophysics, Pennsylvania State University, University Park, PA 16802, USA; E-mail: ggp1@psu.edu
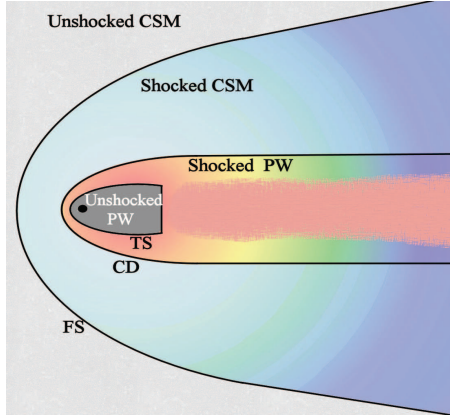
Fig. 1 Cartoon of a head-tail PWN created by a supersonically moving pulsar. A synchrotron (e.g., X-ray) PWN is produced by the shocked PW flowing between the TS and CD surfaces, while the shocked circumstellar medium between the FS and CD surfaces is expected to be the source of IR-optical-UV radiation.

discontinuity (CD) that separates the shocked PW from the shocked ambient medium. Finally, the compressed and heated *shocked ambient medium* between the CD and the forward bow shock (FS) is expected to emit IR-optical-UV radiation in spectral lines and continuum.

For an isotropic pulsar wind, a characteristic distance from the pulsar at which the ram pressure of the unshocked PW, $\dot{E}_w/(4\pi c r^2)$, balances the ram pressure of the ambient medium (the so-called stagnation point) is

$$R_0 = \left(\frac{\dot{E}_w}{4\pi c p_{\mathrm{ram}}} \right)^{1/2} = 1.3 \times 10^{16} \dot{E}_{w,35}^{1/2} n_b^{-1/2} (V_{\mathrm{psr}}/300\,\mathrm{km\,s^{-1}})^{-1}\ \mathrm{cm}, \qquad (2)$$

where $\dot{E}_w = \xi_w \dot{E} = 10^{35} \dot{E}_{w,35}$ erg s^{-1}, $\dot{E}$ is the pulsar's spin-down power, and $\xi_w < 1$ is the fraction of $\dot{E}$ that powers the PW. For an unmagnetized PW, R_0 is approximately equal to the distance of the CD apex ahead of the pulsar, $R_{\mathrm{cd}} \approx R_0$ (van der Swaluw et al. 2004). The characteristic angular separation between the pulsar and the sky projection of the CD surface is

$$\theta_0 \approx R_0/d = 0''\!89\, d_{1.0}^{-1} \dot{E}_{w,35}^{1/2} n_b^{-1/2} (V_{\mathrm{psr}}/300\,\mathrm{km\,s^{-1}})^{-1} \sin i, \qquad (3)$$

where $d = 1.0 d_{1.0}$ kpc is the distance[1], and i is the angle between the line of sight and the pulsar velocity[2]. The small value of θ_0 implies that a subarcsecond resolution (provided only by *Chandra* among the currently active X-ray observatories) is required to resolve the PWN head from the pulsar even for nearby pulsars.

The unshocked PW consists of relativistic particles (likely electrons and positrons) and a magnetic field. The magnetization parameter σ, defined as the ratio of the Poynting flux, $B^2 c/(4\pi)$, to the particle enthalpy flux, is unknown. Pulsar models predict $\sigma \gg 1$ immediately outside the pulsar magnetosphere, while PWN models require $\sigma \lesssim 1$ (or even $\sigma \ll 1$; Kennel and Coroniti 1984) just upstream of the TS. The decrease of σ with distance from the pulsar could be due to transfer of the magnetic field energy to the particles, e.g., by magnetic field reconnection in the striped PW (see Kirk et al. 2009, and references therein). For a given magnetization, the magnetic field upstream of the TS at the stagnation point can be estimated as

$$B \sim \left[\frac{\dot{E}_w \sigma}{c R_0^2 (\sigma+1)} \right]^{1/2} = \left(\frac{4\pi p_{\mathrm{ram}} \sigma}{\sigma+1} \right)^{1/2} \approx 140 \left(\frac{n_b \sigma}{\sigma+1} \right)^{1/2} \frac{V_{\mathrm{psr}}}{300\,\mathrm{km\,s^{-1}}}\ \mu\mathrm{G}. \qquad (4)$$

---

[1] In this Section the subscript of d means the scaling distance in kpc.

[2] Equation 3 is applicable at not too small $\sin i$; see Romani et al. (2010).

The magnetic field can be somewhat higher in the shocked PW, up to a factor of 3 immediately downstream of TS, at $\sigma \ll 1$ (Kennel and Coroniti 1984). Thus, characteristic PWN magnetic field values are expected to be of the order of 10–100 μG.

Typical energies of synchrotron photons emitted in such fields can be estimated as

$$E = \zeta \frac{heB_\perp \gamma^2}{2\pi m_e c} = 1.16\zeta B_{-5}\gamma_8^2 \text{ keV} = 4.43\eta B_{-5}(E_e/100\,\text{TeV})^2 \text{ keV} \qquad (5)$$

where $B_\perp = 10^{-5}B_{-5}$ G is the magnetic field component perpendicular to electron velocity, $\gamma = E_e/(m_e c^2) = 10^8 \gamma_8$ is the electron Lorentz factor, and $\zeta \sim 1$ is a numerical factor. The synchrotron emission spectrum is determined by the electron spectrum, which depends on the still poorly understood acceleration mechanism. The commonly considered Fermi acceleration mechanism at fronts of relativistic shocks (e.g, the TS) gives a power-law (PL) electron spectrum, $dN_e/d\gamma \propto \gamma^{-p}$ in the range $\gamma_{\min} < \gamma < \gamma_{\max}$, with $p \gtrsim 2$ (see, e.g., Chapter 6 of the review by Bykov et al. 2012). Such an electron spectrum produces a PL photon spectrum, $dN/dE \propto E^{-\Gamma}$ in the $E_{\min} < E < E_{\max}$ range, with the photon index $\Gamma = (p+1)/2 \gtrsim 1.5$. The maximum Lorentz factor of accelerated electrons[3], $\gamma_{\max} \lesssim (e/m_e c^2)[\dot{E}\sigma/c(\sigma+1)]^{1/2} \approx 1.1 \times 10^9 \dot{E}_{35}^{1/2}[\sigma/(\sigma+1)]^{1/2}$, can be estimated from the condition $R_g < R_0$, where $R_g = \gamma m_e c^2/(eB) = 1.7 \times 10^{16}\gamma_8 B_{-5}^{-1}$ cm is the gyration radius. This corresponds to the maximum synchrotron photon energy

$$E_{\max} \lesssim 130\zeta \dot{E}_{35}B_{-5}\sigma/(\sigma+1) \text{ keV}. \qquad (6)$$

This equation shows that one should not expect X-ray PWNe from very old, low-power pulsars, but head-tail PWNe could be expected at UV-optical-IR wavelengths.

The qualitative head-tail PWN picture is generally confirmed by analytical estimates (e.g., Romanova et al. 2005) and numerical simulations. For instance, Bucciantini et al. (2005) presented relativistic MHD axisymmetric simulations for $\mathcal{M} = 30$ and three values of the PW magnetization σ upstream of the TS. Figure 1 of that paper shows that for an isotropic PW with a toroidal magnetic field the TS, CD and FS apices are at distances of $\approx R_0$, $1.3R_0$ and $1.7R_0$, respectively, at $\sigma = 0.002$, while the radius of the cylindrical tail (confined by the CD surface behind the pulsar) is $r_{\text{cd}} \approx 4R_0$, almost independent of magnetization. The bulk flow velocity in the tail reaches 0.8–0.9c at its periphery (closer to the CD), being 0.1–0.3c in the central channel (behind the TS bullet). Simulated maps of synchrotron brightness (Figures 4 and 5 in Bucciantini et al. 2005) show that the brightness is maximal at the PWN head, gradually decreasing with distance from the pulsar in the PWN tail.

The inner and outer channels of the tail flow should mix with each other at larger distances from the pulsar due to shear instability. At even larger distances the flow should slow down due to mass-loading of the ambient matter, which leads to additional tail broadening (e.g., Morlino et al. 2015).

As the outflowing electrons lose their energy to synchrotron radiation, we can expect spectral softening with increasing distance from the pulsar, which means the observed tail's length should increase with decreasing photon energy (e.g., it should be larger in the radio than in the X-rays). The length scale of the tail at photon energy E (in keV) can be estimated as

$$l_{\text{tail}} \sim V_{\text{flow}}\tau_{\text{syn}} \sim 18(V_{\text{flow}}/10,000\,\text{km}\,\text{s}^{-1})\zeta^{1/2}E^{-1/2}B_{-5}^{-3/2} \text{ pc} \qquad (7)$$

---

[3]Note that $\gamma_{\max}m_e c^2 \sim e\Phi\sigma/(\sigma+1)$, where $\Phi = B_{\text{LC}}R_{\text{LC}} \sim B_{\text{NS}}R_{\text{NS}}^3\Omega^2/c^2$ is the potential drop across the pulsar's polar cap, $R_{\text{LC}} = c/\Omega$ is the light cylinder radius, $\Omega = 2\pi/P$, B_{LC} and B_{NS} are the magnetic field values at the light cylinder and the neutron star surface. The maximum electron energies in other acceleration models (e.g., Romanova et al. 2005) are also fractions of $e\Phi$.

where $V_{\rm flow}$ is a typical flow velocity and $\tau_{\rm syn} = 1.6\gamma_8^{-1}B_{-5}^{-2}\,{\rm kyr} \sim 1.7\zeta^{1/2}E^{-1/2}B_{-5}^{-3/2}\,{\rm kyr}$ is the synchrotron cooling time. We should note that such an estimate is very crude because both the flow velocity and the magnetic field vary with the distance from the pulsar.

The simulations by Bucciantini et al. (2005) were done for an isotropic PW. We, however, know that at least in some young pulsars the PW is mostly concentrated around the equatorial plane, perpendicular to the spin axis, and the PWN has equatorial and polar components (e.g., the torus and jets in the Crab pulsar; Weisskopf et al. 2000). In this case the ram pressure of the unshocked PW becomes anisotropic, which changes not only the distance to the stagnation point but also the overall PWN appearance. In particular, the PWN shape strongly depends on the angle between the pulsar's velocity and spin vectors, as well as on the angle between the spin vector and the line of sight. Three-dimensional simulations for several cases of anisotropic PW were presented by Vigelius et al. (2007), assuming nonrelativistic, unmagnetized flows (see also Wilkin 2000 and Romani et al. 2010 for analytical approximations). The PW anisotropy should strongly affect the shape of the PWN head, which may become substantially different from the bullet-like one. On the other hand, the shape of tail should not be so strongly affected, especially at large distances behind the pulsar.

In addition to synchrotron (and inverse Compton – see Section ?? [by Matthiey Renaud about TeV PWNe]) emission from the shocked PW, one can expect emission from the shocked ISM, in the region immediately behind the FS. The ambient matter is compressed and heated while passing through the FS, up to ion temeperatures

$$T_i = (3/16)(\mu_i m_p/k)V_{\rm psr}^2 = 2 \times 10^6 \mu_i (V_{\rm psr}/300\,{\rm km\,s}^{-1})^2\,{\rm K}, \qquad (8)$$

where $\mu_i m_p$ is the mean ion mass. Behind the FS front the energy of ions is partly transferred to electrons, which emit in both continuum and spectral lines in the optical, UV, and even soft X-ray ranges. If there are neutral hydrogen atoms in the ambient medium ahead of the pulsar, they can be excited at the FS and emit spectral lines in the course of radiative de-eexcitation.

Thus, a rotation-powered pulsar that has left its parent SNR should be accompanied by a nebula that consists of a head-tail synchrotron component, emitting in a broad energy range, perhaps from the radio to soft γ-rays, enveloped by a (forward) bow-shock component observable in the optical-UV (particularly, in the Balmer lines). Below we will see, however, that observational results do not always coincide with the predictions of the current simple models.

1.2 Observational results

Although most of the known rotation-powered pulsars have left their SNRs and are moving with supersonic velocities, their spin-down powers (hence the PWN luminosities) have significantly decreased with age. Therefore, the number of detected head-tail (bow-shock) PWNe is relatively small. Among over 70 PWNe detected in X-rays (Kargaltsev et al. 2013) only about 15 PWNe are created by old (and/or fast) enough pulsars that have left their parent SNRs, with spin-down powers $0.012 \lesssim \dot{E}_{35} \lesssim 26$ and characteristic (spin-down) pulsar ages $\tau_{\rm sd} \gtrsim 20$ kyr. An even smaller number of head-tail PWNe were observed with exposures deep enough to accurately measure the X-ray PWN properties. Below we present a few examples of such observations.
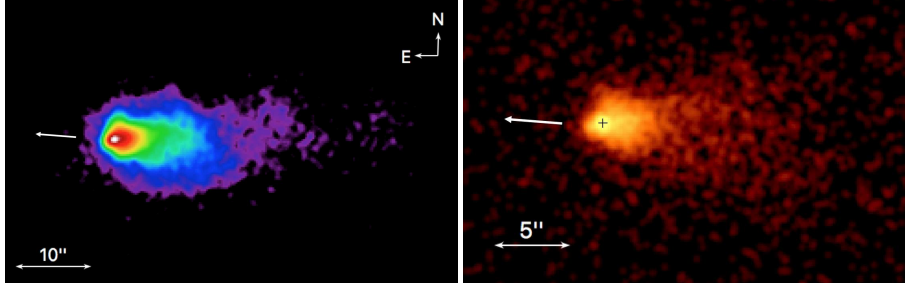
Fig. 2 Left: Merged image from 5 *Chandra* ACIS observations of the Mouse (0.5–8 keV, 154 ks exposure). Right: *Chandra* HRC image of the Mouse (58 ks exposure). The cross in the right image marks the pulsar position, the arrows show the direction of proper motion.
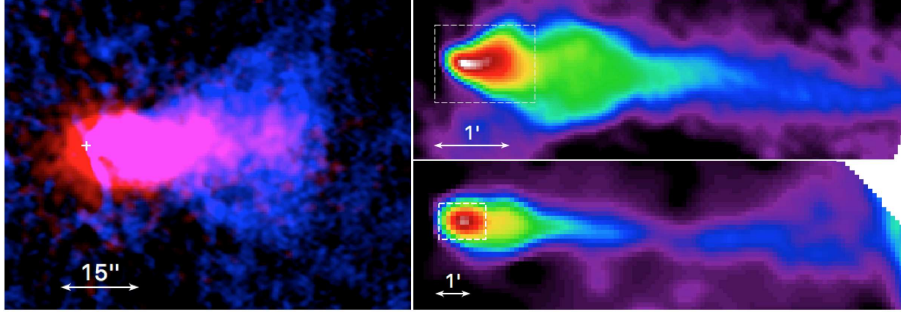

Fig. 3 Left: Composite X-ray (red; ACIS) and radio (blue; VLA, 1″07 beam) image of the Mouse PWN. The pulsar position is shown by the white cross. Right: VLA radio images (top: 11″ beam, bottom: 32″ beam) showing the extended tail of the Mouse. The field of view of the left image is shown by the dashed white boxes in the right panels. The radio images were obtained from the NRAO VLA Archive.

1.2.1 The Mouse: A textbook example?

The Mouse PWN was discovered in a radio survey of the Galactic center region (Yusef-Zadeh and Bally 1987). The VLA image showed a bright compact head ("snout"), a bulbous $\sim 2'$ long "body", and a remarkably long, $\sim 12'$, narrow "tail" (see the right panels in Figure 1.2.1). Camilo et al. (2002) discovered a 98 ms pulsar, J1747–2958, within the Mouse's head, with a spin-down power $\dot{E} = 2.5 \times 10^{36}$ erg s^{-1} and a characteristic age $\tau_{\mathrm{sd}} = 25$ kyr. Hales et al. (2009) measured the proper motion of the radio PWN head[4], $\mu = 12.9 \pm 1.8$ mas yr^{-1}, which corresponds to a transverse velocity $V_\perp = (306 \pm 43)d_5$ km s^{-1}, where $d_5 = d/5$ kpc. Based on the projected tail length, $\sim 17d_5$ pc, and the lack of an SNR that could possibly be associated with the pulsar (see, however, Yusef-Zadeh and Gaensler 2005), Hales et al. (2009) argue that the true age of the pulsar is $\gtrsim 160$ kyr.

The Mouse PWN was observed with *Chandra* by Gaensler et al. (2004) and Klingler et al. (2017, in prep), with 36 ks and 120 ks exposures, respectively. These observations have shown an X-ray nebula with a compact bright head and a tail of $\sim 45''$ length, a factor of 16 shorter than the radio tail (see Figure 1.2.1). The X-ray luminosity of the PWN, $L_{0.5-8\,\mathrm{keV}} \approx 3.3 \times 10^{34} d_5^2$ erg s^{-1}, is about $0.013 d_5^2$ of the pulsar's spin-down power, un-

---

[4]It can differ from the pulsar's proper motion if the pulsar moves in a non-uniform ambient medium, but we will neglect this difference here.
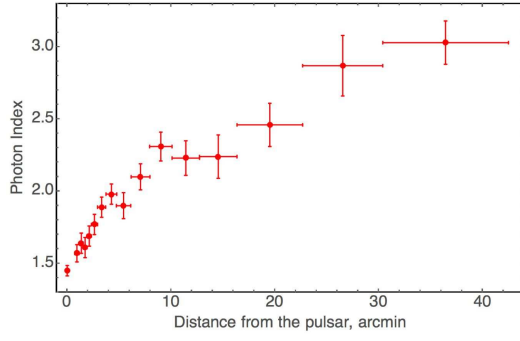
Fig. 4 Photon index Γ as a function of distance from the pulsar along the tail of the Mouse (Klingler et al. 2017, in prep.).

usually high compared to other PWNe (Kargaltsev and Pavlov 2008). The distance from the pulsar to the projected leading edge of the head, $\theta_0 \approx 1''$, corresponds to $n_b \sim 0.8\xi_w d_5^{-4}\sin^2 i$ cm^{-3} (see Equation 3), typical for a warm phase of the ISM. For a sound speed of ~ 10 km s^{-1}, expected for this phase, the pulsar's Mach number can be estimated as $\mathcal{M} \sim 30d_5/\sin i$. The spatially-resolved X-ray spectrum showed a significant increase of the photon index with increasing distance from the pulsar, from $\Gamma \approx 1.6$ in the immediate vicinity of the pulsar to $\Gamma \approx 3.0$ at $\sim 40''$ from the pulsar (see Figure 1.2.1). Interpreted as synchrotron cooling, this softening requires a strong magnetic field of a few hundreds μG, assuming equipartition between the magnetic field energy and the kinetic energy of relativistic electrons. The projected length of the X-ray tail, $l_{\text{tail}} \sim 1d_5$ pc, corresponds to the flow velocity $V_{\text{flow}} \sim 20{,}000 B_{-4}^{3/2} d_5/\sin i$ km s^{-1}, much higher than V_{psr} but significantly lower than the mildly relativistic speeds predicted by Bucciantini et al. (2005). Moreover, the comparison of the X-ray and high-resolution radio images (see the left panel of Figure 1.2.1) suggests that the flow is faster in the middle of the tail, contrary to the model predictions.

The radio tail of the Mouse is longer than in any other known PWN. Just behind the pulsar, the radio image looks like a cone with an $\approx 25°$ half-opening angle (much broader than the Mach cone at the above-estimated $\mathcal{M} \sim 30$) and a vertex at the pulsar position. The cone abruptly narrows at $\sim 1'$ from the pulsar. Such behavior is not explained by the current PWN models. The Mouse is one of the few PWNe with a mapped radio polarization. Polarization mesurements by Yusef-Zadeh and Gaensler (2005) suggest that the magnetic field wraps around the bow shock structure near the apex of the system, but runs parallel to the direction of the pulsar's motion in the tail behind the pulsar. Such a magnetic field distribution is different from the toroidal one assumed in the models by Bucciantini et al. (2005). Thus, the Mouse has a few features consistent with the model predictions, but the models do not fully agree with the observations, particularly in the radio.

1.2.2 Geminga: An odd "three-tail" PWN

The X-ray PWN created by the radio-quiet γ-ray pulsar Geminga ($P = 237$ ms, $\dot{E} = 3.3 \times 10^{34}$ erg s^{-1}, $\tau_{\text{sd}} = 340$ kyr, $d = 0.25^{+0.23}_{-0.08}$ kpc) looks quite different from the Mouse[5] and from the predictions of PWN models. The proper motion of this pulsar, $\mu = 178.2 \pm 1.8$ mas yr^{-1} (Faherty et al. 2007), corresponds to the transverse velocity $V_\perp = (211 \pm 2)d_{0.25}$ km s^{-1}. Observations with *XMM-Newton* revealed two bent "tails" behind the pulsar, on both

---

[5] One should bear in mind, however, that much smaller spatial scales can be probed in the nearby Geminga PWN than in the Mouse.
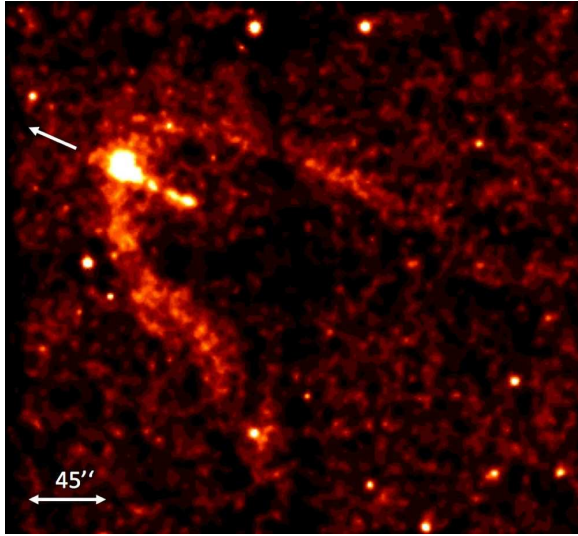
Fig. 5 Combined *Chandra* ACIS image of the Geminga PWN (0.5-8 keV, 540 ks). The arrow shows the direction of pulsar's proper motion.

sides of its sky trajectory (Caraveo et al. 2003), while *Chandra* observations with a higher spatial resolution showed a shorter third tail between the two lateral tails (Pavlov et al. 2006; Pavlov et al. 2010). The most detailed data on the Geminga PWN were provided by a series of 12 *Chandra* observations carried out in 2012–2013, with a total exposure of about 580 ks Posselt et al. (2016). Figure 1.2.2 shows a summed image from these observations, where we see two lateral tails of $\sim 3'$ ($0.2d_{0.25}$ pc) length and one $\sim 0.45''$ ($0.05d_{0.25}$ pc) long central tail. Surprisingly, there is only a hint of bow-like emission ahead of the pulsar and no bright, filled 'bullet' predicted by the PWN models assuming an isotropic PW. The 0.3–8 keV luminosities of the northern and southern lateral tails, and the central tail are 1.6, 2.6, and $0.9 \times 10^{29}d_{0.25}^2$ erg s^{-1}, respectively, i.e., the total PWN luminosity is a fraction of $1.5 \times 10^{-5}d_{0.25}^2$ of the pulsar's spin-down power, two orders of magnitude smaller than for the Mouse. Images from separate exposures show that the central tail is formed by isolated "blobs" seen at different distances from the pulsar in different observations (see Figure 1.2.2). However, there is no evidence of constant or decelerated motion of the blobs. The spectra of the lateral tails are very hard, $\Gamma \approx 0.7$–1.0, much harder than the spectrum of the central tail, $\Gamma \approx 1.6$, and they do not show significant changes with increasing distance from the pulsar.

The nature of the three tails is not certain yet. One could assume that the lateral tails represent a limb-brightened paraboloid shell of shocked PW downstream of the TS and their unusually hard spectrum is emitted by electrons accelerated by the Fermi mechanism at the shocks that form in two colliding flows (in the reference frame of CD) – the PW and the oncoming ambient medium. However, a lack of diffuse emission in between the lateral tails strongly suggests that the shell emissivity is not azimuthally symmetric with respect to the shell axis (i.e., the direction of motion). Such an asymmetry could be caused by a strong asymmetry of the PW (e.g., because the equatorial plane around the pulsar spin axis, where the PW is presumbly concntrated, is strongly misaligned with the direction of motion) or an azumuthally asymmetric magnetic field in the shell (see Posselt et al. 2016 for details). Alternatively, the lateral tails could be interpreted as strongly collimated polar outflows (jets) bent by the ram pressure of the oncoming ambient medium. The blobs in
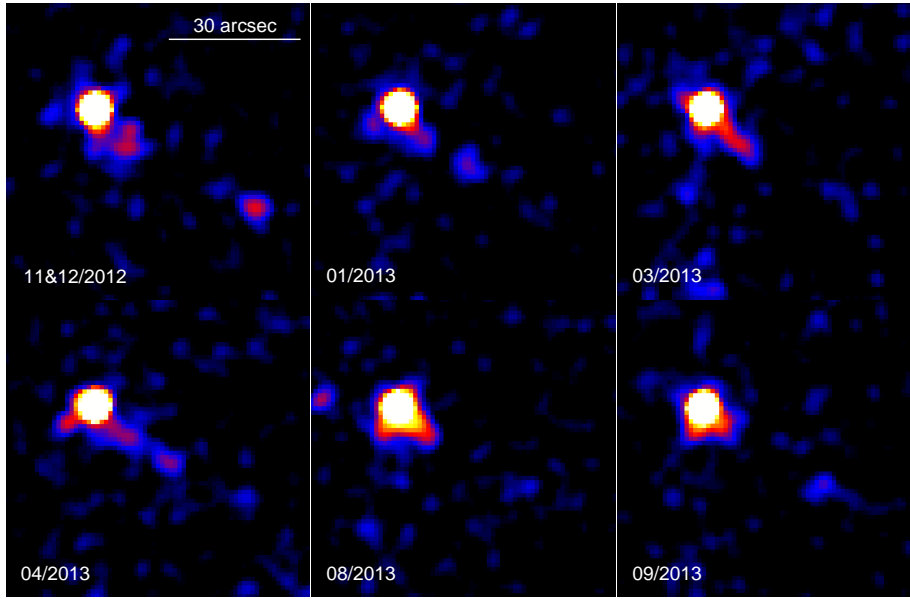
Fig. 6 Images of the central tail of the Geminga PWN in separate *Chandra* observations.

the central tail could be short-lived plasmoids formed by magnetic field reconnection in the relativistic plasma behind the moving pulsar, resembling the magnetotails of the Solar system planets. Observations at different wavelengths could clarify the PWN nature, but the Geminga PWN was not detected in the radio or Hα. At any interpretation, we can conclude that the Geminga's PW is strongly anisotropic, and new models are required to explain the the morphologies and spectra of such PWNe.

1.2.3 The Guitar: First example of a misaligned outflow

The Guitar nebula is produced by the relativly old, low-power pulsar B2224+65 ($P = 683$ ms, $\dot{E} = 1.2 \times 10^{33}$ erg s^{-1}, $\tau_{sd} = 1.12$ Myr). The pulsar is among the highest velocity neutron stars known; its proper motion, $\mu = 182 \pm 3$ mas yr^{-1}, corresponds to the transverse velocity $V_\perp = 860$–1730 km s^{-1} (the uncertainty is caused by the uncertain distance, $d = 1$–2 kpc). The guitar-shaped Hα nebula was discovered by Cordes et al. (1993) and further studied in several papers (see Dolch et al. 2016 and references therein). One could expect a head-tail X-ray PWN within the Hα bow shock, but a high-resolution observation with *Chandra* showed instead a straight $2'$ ($0.3d_1$ pc) long feature inclined by $118°$ to the direction of the pulsar's proper motion (Wong et al. 2003; Hui and Becker 2007; see Figure 1.2.3). A second *Chandra* observation 6 years later showed that the sharp leading edge of the jet-like feature had the same proper motion as the pulsar, and it provided evidence for the presence of a counter-feature, albeit substantially shorter and fainter than the main one (Johnson and Wang 2010). The feature shows a power-law spectrum with $\Gamma \approx 1.6$, comparable to that of the point-like source (the pulsar plus an unresolved PWN?). The luminosity of the feature, $L_{0.3-7\text{keV}} \sim 7 \times 10^{30} d_1^2$ erg s^{-1}, exceeds that of the point-like source by a factor of 3–4, and is a fraction of $\sim 6 \times 10^{-3} d_1^2$ of the pulsar's spin-down power.
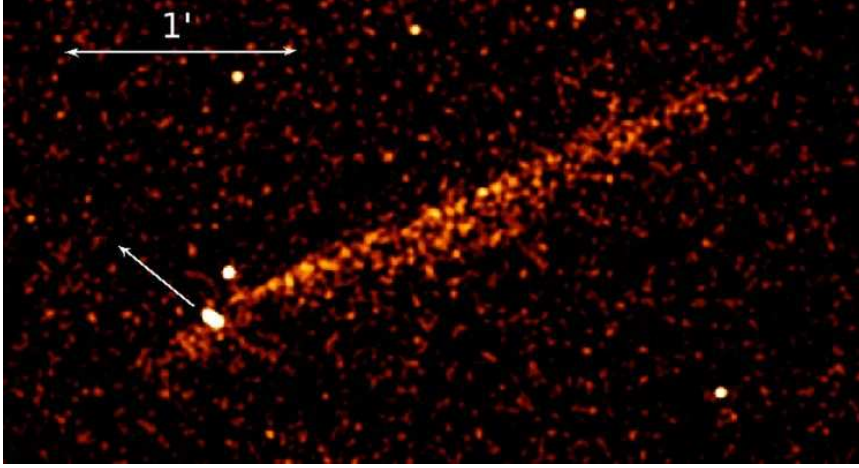
Fig. 7 *Combined Chandra* ACIS image (0.5–8 keV, 195 ks total exposure) of PSR B2224+65 and its misaligned outflow.

The lack of a resolved X-ray head-tail PWN could be explained by the very high pulsar velocity and low spin-down power. Indeed, according to Equation 2, the characteristic PWN size ahead of the pulsar, $R_0 \sim 5 \times 10^{14} \xi_w^{1/2} n_b^{-1/2} d_1^{-1}$ cm, correponds to the angular distance[6] as small as $\theta_0 \sim 0''03 (\xi_w/n_b)^{1/2} d_1^{-2}$, much smaller than the angular resolution of *Chandra*. The lack (shortness) of the X-ray tail could be due to a high magnetic field (hence fast synchrotron cooling) in the shocked PW associated with the small stand-off distance (see Equation 4). Another reason could be a low maximum energy of accelerated electrons at the low spin-down power of B2224+65 (see Equation 6).

The nature of the elongated feature remains unclear. It might be a pulsar jet, but such a jet should be bent by the ram pressure of the oncoming ambient medium while no bending is observed. Bandiera (2008) suggested that the feature is produced by synchrotron radiation of highest energy electrons ($\gamma \sim 10^8$) accelerated at the TS and leaked into the ISM along its magnetic field. This scenario, however, requires a rather high ambient magnetic field ($\sim 45\,\mu$G, according to Bandiera 2008) and it remains unclear why the counter-feature is so much fainter than the main one. Since the true nature of the feature is not certain yet, we will call it simply a *misaligned outflow*. It should be emphasized that, most likely, the misaligned outflow is not a (magneto)hydrodynamical flow but rather a stream of high-energy particles not interacting with each other and with the ISM gas.

1.2.4 J1509–5850: Another misaligned outflow, a "three-tail" compact nebula, and a long tail

PSR J1509–5850 is a middle-aged ($\tau_{sd} = 154$ kyr) pulsar with $P = 89$ ms, $\dot{E} = 5.1 \times 10^{35}$ erg s^{-1}, and a dispersion-measure distance $d \approx 3.8$ kpc. Its X-ray PWN, consisting of a compact "head" and a long "tail" southwest of the pulsar, was discovered in a *Chandra* observation by Kargaltsev et al. (2008). Deep follow-up *Chandra* observations (374 ks total exposure) are described by Klingler et al. (2016a). In addition to the previously detected

---

[6]Chatterjee and Cordes (2002) estimated $\theta_0 = 0''06 \pm 0''02$ from modeling an Hα image obtained with the *Hubble Space Telecope*.
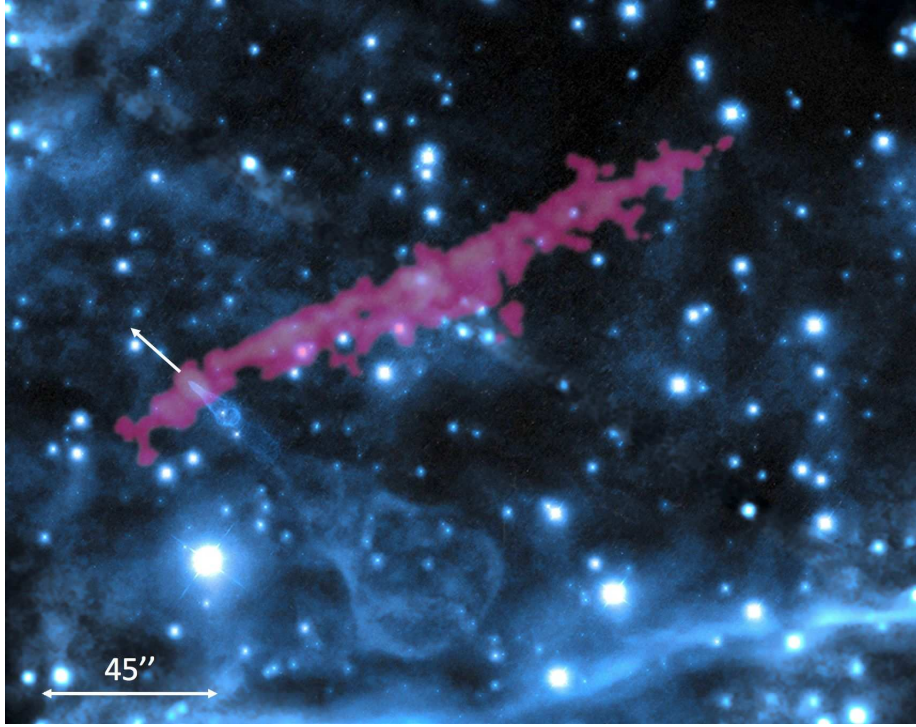
Fig. 8 Smoothed X-ray image from Figure 1.2.3 overlaid onto the Hα image showing the Guitar. The Hα image is taken from http://chandra.harvard.edu/photo/2015/archives/.

southwest tail extending up to $7'$ ($7.7d_{3.8}$ pc), these observations revealed similarly long (but fainter) diffuse emission stretched toward the north and the fine structure of the PWN "head" (see Figure 1.2.4). The "head" (dubbed the Compact Nebula [CN] by Klingler et al. 2016a) is resolved into two lateral tails and one short central tail (Figure 1.2.4), remarkably similar to the Geminga PWN. Although the pulsar's proper motion has not been measured, the overall CN and southwest tail morphology provides strong evidence that the pulsar is moving northeast. In this case the northern structure is another example of a misaligned outflow.

Klingler et al. (2016a) estimated upper and lower limits for the transverse velocity, $V_\perp \lesssim 640d_{3.8}$ km s^{-1} and $V_\perp \gtrsim 160n_b^{-1/2}d_{3.8}^{-1}$ km s^{-1}, using upper limits on the pulsar's proper motion and stand-off distance (the latter estimate assumes an isotropic PW). Being morphologically similar to the Geminga PWN, the CN of J1509–5850 is a factor of ~ 200 more luminous (e.g., $L_{0.5-8\,\mathrm{keV}} \approx 7.5 \times 10^{31}d_{3.8}^2$ erg s^{-1} for the CN lateral tails) and a factor of ~ 10 more X-ray efficient ($\eta_{0.5-8\,\mathrm{keV}} \equiv L_{0.5-8\,\mathrm{keV}}/\dot{E} \approx 1.5 \times 10^{-4}d_{3.8}^2$ vs. $1.5 \times 10^{-5}d_{0.25}^2$ for Geminga). In addition, the spectra of the lateral tails are much softer in the CN than in the Geminga PWN ($\Gamma \approx 1.8$ vs. $\Gamma \approx 1$, respectively). The reason of these differences is currently unclear.

Being aligned with the CN symmetry axis, the extended tail southwest of the pulsar is obviously composed of a shocked PW collimated by the ram pressure. Its luminosity is $L_{0.5-8\,\mathrm{keV}} \approx 1 \times 10^{33}d_{3.8}^2$ erg s^{-1}, and its spectral slope, $\Gamma \approx 1.9$, does not show any increase (rather a hint of decrease) with increasing distance from the pulsar. The lack of spectral
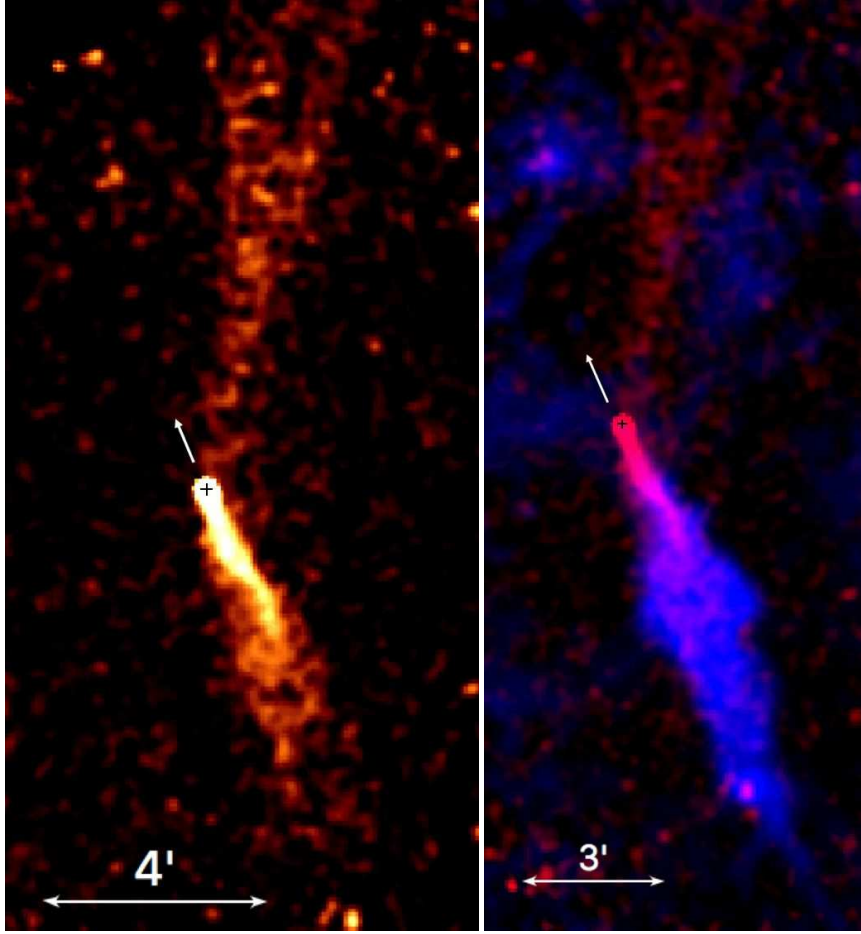
Fig. 9 Left: *Chandra* ACIS image of the J1509–5850 PWN (0.5–8 keV, 374 ks) showing the southwest tail and the misaligned outflow toward the north. Right: Combined *Chandra* ACIS (red) and VLA (blue) image of the same PWN. The arrows show an assumed direction of proper motion.

softening suggests a very high speed of the outflowing matter. Alternatively, there could be some "reheating" due to in situ conversion of magnetic field energy into particle energy, e.g., via turbulent processes and accompanying reconnection, which might explain the hint of spectral hardening at large distances from the pulsar. The tail is also seen in radio up to about $10'$ from the pulsar (Ng et al. 2010). Surprisingly, the radio emission brightens with distance from the pulsar (contrary to the Mouse tail), becomes broader than the X-ray emission beyond $\approx 3'$, and then narrows again beyond $\approx 5'$ (see Figure 1.2.4). Another difference from the Mouse tail is the predominant magnetic field orientation, stretched along the tail in the Mouse and helical, with the helix axis parallel to the pulsar's direction of motion, in the J1509 tail. The different magnetic field geometries possibly reflect different spin-velocity alignments of the parent pulsars.

The median of the $7'$ long wedge-like northern structure is inclined to the CN symmetry axis (alleged direction of proper motion) by $\approx 33°$. Its luminosity, $L_{0.5-8\,\mathrm{keV}} \approx 4 \times 10^{32} d_{3.8}^2$,
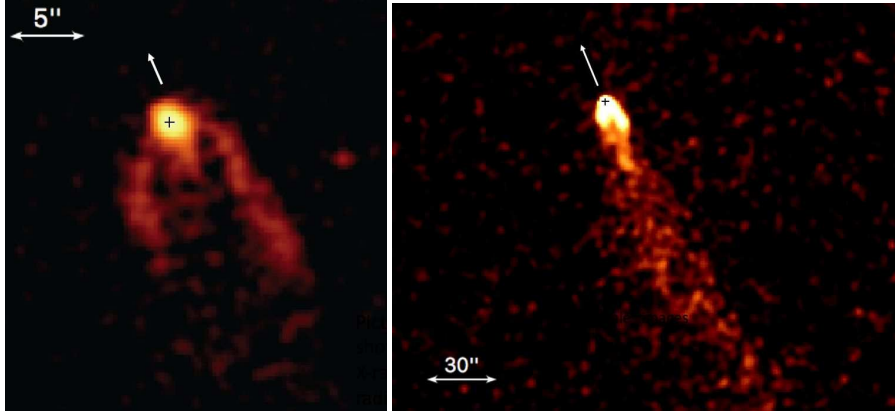
Fig. 10 Left: Compact X-ray nebula in the vicinty of PSR J1509–5850. Right: ACIS image demonstrating the transition from the compact nebula to the southwest tail.

is a factor of 2.5 lower than that of the southwest tail, while the spectral slope is about the same, with a slight hint of softening with increasing distance from the pulsar.

1.2.5 The complex PWN created by PSR B0355+54

PSR B0355+54, located at a parallax distance of $d = 1.0 \pm 0.2$ kpc, is a middle-aged radio pulsar ($\tau_{sd} = 560$ kyr) with a spin-down power $\dot{E} = 4.5 \times 10^{34}$ erg s^{-1} and a period $P = 156$ ms. Its transverse velocity, $V_\perp = 61^{+12}_{-9} d_1$ km s^{-1} towards the northeast, is among the lowest observed. Observations with *Chandra* and *XMM-Newton* revealed the presence of a PWN (dubbed the Mushroom by Kargaltsev and Pavlov 2008) consisting of a compact "cap" and a dimmer "stem", with a hint of extended emission visible up to $\sim 7'$ (2 pc) southwest of the pulsar (McGowan et al. 2006). A series of 8 *Chandra* observations, performed over an 8 months period in 2012-2013 (total exposure of 395 ks) revealed the detailed structure of the B0355+54 PWN (see Figure 1.2.5) and allowed us to measure the spectra of its elements (Klingler et al. 2016b). In particular, they showed a "filled" morphology of the cap, in contrast with the "hollow" morphologies of the Geminga PWN and the CN of the J1509–5850 PWN. The cap has a sharp trailing edge behind the pulsar and is brightened along the axis; its spectral slope is $\Gamma \approx 1.5$, a typical value for a PWN head. The stem is split into two structures that apparently originate from the pulsar and slightly diverge from each other further away. Klingler et al. (2016b) speculate that these structures could be pulsar's jets swept back by the ram pressure, which could also explain the brightening along the cap's axis. Overall, the "mushroom" morphology suggests a small angle between the pulsar's spin axis and our line of sight, in agreement with the lack of γ-ray pulsations. The cap and stem luminosities are 1.8×10^{31} and 2.6×10^{30} erg s^{-1}, respectively.

A long diffuse tail behind the "mushroom" is likely due to synchrotron emission of the shocked PW behind the pulsar. Its luminosity is about 3.8×10^{31} erg s^{-1}, more than a half of the total PWN luminosity, $L_{0.5-8\,keV} \approx 6.4 \times 10^{31}$ erg s^{-1} that corresponds to a total PWN efficiency $\eta_{0.5-8\,keV} \approx 1.4 \times 10^{-3}$. The spectrum of the tail, with a slope $\Gamma \sim 1.7$–1.8, shows only a slight hint of cooling with increasing distance from the pulsar. This implies either a a fast flow speed (or a very low magnetic field), or particle re-acceleration within the tail.
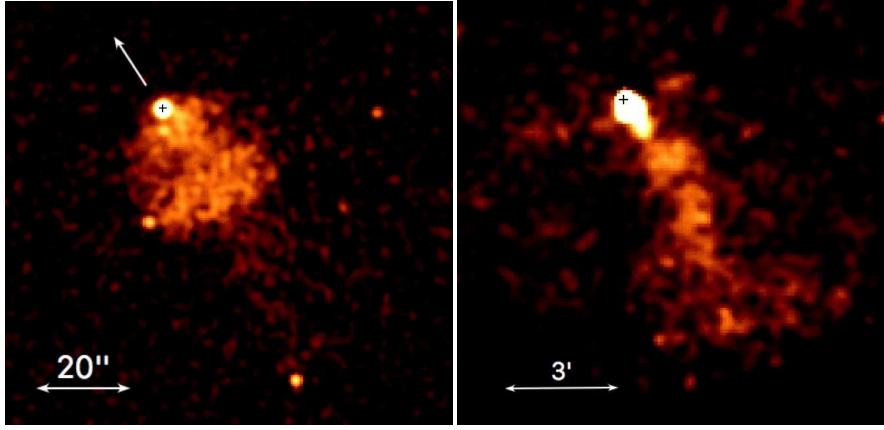
Fig. 11 *Chandra* ACIS images of the B0355+54 PWN (0.5–8 keV, 395 ks). Left: The compact PWN in the pulsar vicinity (the Mushroom). Right: The large-scale PWN, including the diffuse tail and the "whiskers". The arrows show the direcion of the proper motion.

The deep observation also allowed Klingler et al. (2016b) to detect two additional very faint, extended features (dubbed "whiskers") on either side of the compact nebula, likely another example of a misaligned outflow.

Thus, the B0355+54 PWN shows a particularly rich structure, which remains to be explained by PWN models. Radio and Hα observations could shed light on its nature, but the PWN has not been detected at these wavelengths.

1.2.6 J1741–2054: Another tail behind a nearby middle-aged pulsar

Another example of a tail-like structure behind a moving pulsar is shown in Figure 1.2.6. This PWN was discovered by Romani et al. (2010) and investigated in detail by Auchettl et al. (2015) using results from 6 *Chandra* observations carried out in 2013 (282 ks total exposure) . It is created by the nearby ($d \sim 0.38$ kpc) middle-aged ($\tau_{\mathrm{sd}} = 390$ kyr) pulsar J1741–2044 ($P = 413$ ms, $\dot{E} = 9.5 \times 10^{33}$). The pulsar's proper motion $\mu = 109 \pm 10$ mas yr^{-1}, measured by Auchettl et al. (2015) from the X-ray images, corresponds to the transverse velocity $V_{\perp} = (196 \pm 18)d_{0.38}$ km s^{-1}. In Figure 1.2.6 we see a tail-like structure in the direction opposite to that of the proper motion. The structure consists of a compact elongated nebula of $\sim 15''$ length and a fainter diffuse tail seen up to $\sim 1\!.\!7$ ($\sim 0.2d_{0.38}$ pc) from the pulsar. The tail is slightly bent and apparently consists of two "lobes". No small-scale structure (PWN head) is resolved around the pulsar. The 0.5–10 keV luminosities of the compact nebula and the entire PWN, about 5×10^{29} and 3×10^{30} erg s^{-1} at $d = 0.38$ kpc, are $\sim 5 \times 10^{-5}$ and $\sim 3 \times 10^{-4}$ of the pulsar's spin-down power. The spectra of the PWN elements are described by a PL model with $\Gamma \approx 1.5$–1.7, with only a hint of spectral softening with increasing distance from the pulsar.

For an isotropic PW, one could expect a PWN head with a leading edge at an angular distance $\theta_0 \approx 1'' d_{0.38}^{-2} n_b^{-1/2} \sin i$ ahead of the pulsar, too small to resolve it from the pulsar's PSF. The actual distance to the stagnation point is likely even smaller, as seen from the Hα image (see Figure 1.2.6). The flat front of the Hα bow shock allows one to assume that the wind of this pulsar is originally concentrated in the plane perpendicular to the pulsar's velocity, presumably the equatorial plane, which implies that the pulsar's rotational axis is
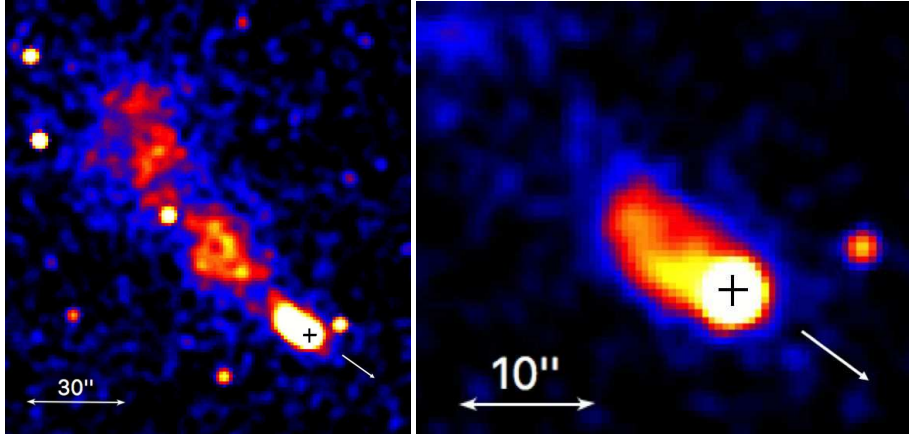
Fig. 12 Summed 0.3–6 keV *Chandra* ACIS images of the entire J1741–2054 PWN (left) and the leading bright component (right) from 5 observations in 2013 (282 ks total exposure). Black crosses show the pulsar position, white arrows show the direction of proper motion.
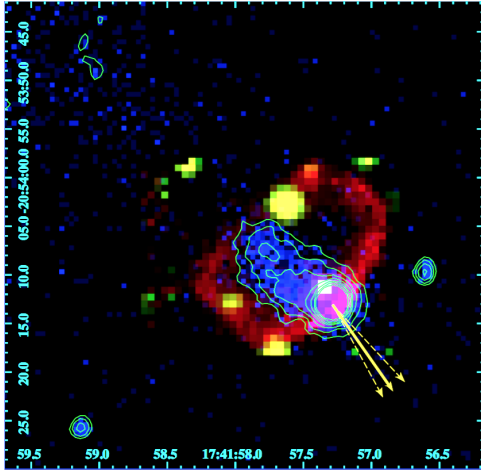

Fig. 13 The Hα nebula (red) and the leading tail component of the X-ray PWN created by PSR J1741–2051 (Auchettl et al. 2015)

.

parallel to the velocity vector. Being deflected by the ram pressure, the shocked PW forms the tail seen as a brighter compact component (Figure 1.2.6, right). The matter flowing in the tail is likely decelerated by the ISM entrainment, which leads to the broadening seen in the diffuse longer tail. To confirm this interpretation, flow velocities in the compact and extended tail components should be measured, but it was not possible with the data available.

1.2.7 J0357+3205: A tail detached from the pulsar

An interesting X-ray nebula created by a radio-quiet γ-ray pulsar J0357+3205 ($P = 444$ ms, $\tau_{sd} = 540$ kyr, $\dot{E} = 5.9 \times 10^{33}$ erg s^{-1}) is shown in Figure 1.2.7 (De Luca et al. 2011). The pulsar's proper motion is $\mu = 164 \pm 20$ mas yr^{-1} (De Luca et al. 2013), but the distance is unknown. For an assumed $d = 0.5$ kpc, its transverse velocity is $V_\perp = (389 \pm 47)d_{0.5}$
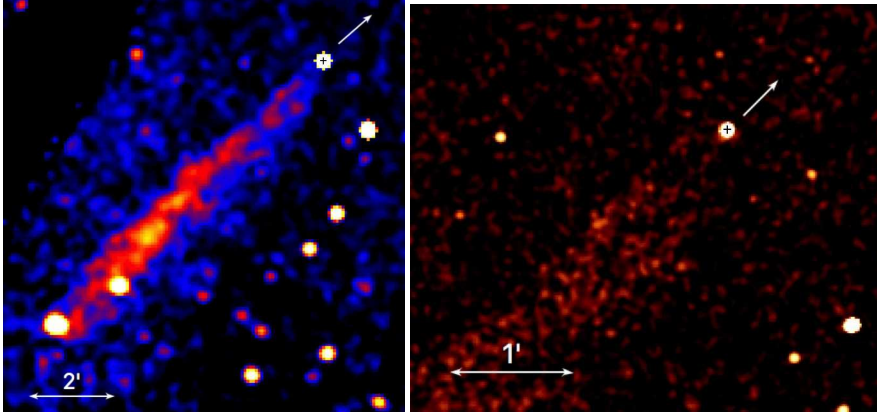
Fig. 14 Left: Merged *Chandra* ACIS image of the tail behind PSR J0357+3205 (0.5–6 keV, 4 observations, 136 ks total exposure). Right: Zoomed-in part of the same image showing the lack of tail emission in the pulsar vicinity.

km s^{-1}. The *Chandra* and *XMM-Newton* images show a $9'$ ($1.3d_{0.5}$ pc) long, relatively straight tail behind the pulsar, but no PWN head is seen. Moreover, the tail is detached from the pulsar (not seen up to $50''$), and its brightness increases with increasing distance from the pulsar, reaching a maximum at about $4'$. Another unusual property of the tail is the asymmetric brightness profile across the tail, with a sharp northeastern edge, resembling the "misaligned outflow" in the Gutar nebula. The tail's luminosity, $L_{0.5-10\,\mathrm{keV}} \approx 8.8 \times 10^{30} d_{0.5}^2$ erg s^{-1}, is a fraction of $\sim 1.5 \times 10^{-3}$ of the pulsar's spin-down power.

The tail's spectrum fits a PL model with a photon index $\Gamma \approx 2$, without a significant dependence on the distance from the pulsar. Such a spectrum is consistent with the synchrotron emission from relativistic electrons in a shocked PW, but the lack of a PWN head is challenging for such an interpretation. Another potential problem is the relatively low value for the maximum synchrotron photon energy, $E_{\max} \lesssim 30 \eta \sigma B_{-5}$ keV (see Equation 6), which is below 1 keV if $\eta \sigma B_{-5} \lesssim 0.03$. To circumvent these problems, Marelli et al. (2013) suggest that the tail's emission is in fact a thermal bremsstrahlung from the shocked ISM material with a temperature of about 4 keV. To heat the ISM up to such a high temperature, a very high pulsar velocity, $V_{\mathrm{psr}} \sim 1900$ km s^{-1}, is required (see Equation 8), larger than observed for any other pulsar, which would also imply a small angle, $i < 20°$, between the velocity vector and the line of sight. The lack of diffuse emission at small distances from the pulsar could then be caused by a considerable time required for the energy transfer from ions, heated by the shock, to radiating electrons. If this scenario is confirmed by future observations, the J0357+3205 nebula would be the first example of a new class of thermally emitting nebulae associated with high-velocity pulsars.

1.2.8 Unexpectedly faint X-ray PWNe

From the above examples one could expect that any sufficiently powerful pulsar that has left its parent SNR produces a head-tail PWN, possibly with some misaligned outflows. However, observations of several nearby pulsars show either very faint extended emission around the pulsar or no extended emission at all. The most convincing examples of very faint (or undetected) PWNe were provided by observations of nearby pulsars B1055–52 and B0656+14.

PSR B1055–52 ($P = 197$ ms, $\dot{E} = 3.0 \times 10^{34}$ erg s^{-1}, $\tau_{sd} = 535$ kyr) is a bright γ-ray pulsar at an estimated distance of ~ 350 pc (Mignani et al. 2010). Its proper motion, $\mu = 42 \pm 5$ mas yr^{-1}, corresponds to the tranverse pulsar velocity $V_\perp \approx 70 d_{0.35}$ km s^{-1}. A dedicated 56 ks *Chandra* ACIS observation by Posselt et al. (2015) showed some enhancement (with respect to the model PSF) in radial count distribution from $2''$ to $20''$, better seen in the soft X-ray band (0.3–1 keV), corresponding to the luminosity of $1–2 \times 10^{29} d_{0.35}^2$ erg s^{-1}, which is $(3–6) \times 10^{-6} d_{0.35}^3$ of the pulsar's spindown power. The alleged extended emission showed only a hint of azimuthal asymmetry (an excess in the quadrant that includes the proper motion direction), at a 3σ level. This extended emission (if real) could be, at least partly, a dust scattering halo, but a very faint X-ray PWN cannot be excluded. Posselt et al. (2015) speculate that such a faint, nearly round PWN could be produced if the pulsar is moving away from us almost along the line of sight, i.e., $V_{psr} \gg V_\perp$. It, however, remains unclear whether this interpretation is correct.

Very similar results were obtained by Bîrzan et al. (2016) for PSR B0656+14 ($P = 385$ ms, $\dot{E} = 3.8 \times 10^{34}$ erg s^{-1}, $\tau_{sd} = 111$ kyr, and $d = 0.29 \pm 0.03$ kpc from parallax measurements). This pulsar also has a low transverse velocity, $V_\perp = (60 \pm 7) d_{0.29}$ km s^{-1}. From the analysis of archival *Chandra* ACIS and HRC data, Bîrzan et al. (2016) found a slight enhancement over the model PSF in an annulus of about $3''$–$15''$ around the pulsar, with a luminosity of $\sim 8 \times 10^{28} d_{0.29}^2$ erg s^{-1}. This luminosity is $\sim 2 \times 10^{-6} d_{0.29}^2$ of the pulsar's spindown power, a factor of ~ 7 lower than the X-ray efficiency of the PWN of Geminga that has a similar (slightly higher) spindown power and is a factor of 3 older than PSR B0656+14. No azimuthal asymmetry was detected in the images. The spectrum of the enhancement is apparently very soft, $\Gamma \sim 8$, but its uncertainty is very large because the imaging ACIS observation was very short, about 5 ks. Similar to B1055–52, the extended emission (if real) could be a combination of a dust scattering halo and a PWN created by the pulsar moving almost along the line of sight. The PWN and halo contributions could be disentangled from a longer ACIS observation.

Thus, a plausible explanation for the lack of the expected head-tail morphology and a very low PWN luminosity might be due to smallness of the angle between the pulsar velocity direction and the line of sight, which is also indicated by the small values of $V_\perp$. However, the transverse velocity of PSR B0355+54 is similarly low, but that pulsar is accompanied by a PWN with a rich structure (see Figure 1.2.5). Moreover, the spindown power of PSR B0355+54 is similar to those of B1055–52 and B0656+14, but its PWN luminosity is at least a factor of 300 higher. Obviously, there should be some other factors that affect the X-ray efficiency and appearance of PWNe created by pulsars moving in the ISM. A possible reason for these differences could be different orientations of the pulsar rotational axes (hence the equatorial planes) with respect to their velocities. Another parameter on which the PWN properties should depend is the angle between the spin and magnetic axes, which affects the conversion of the PW magnetic energy into the kinetic energy and the particle acceleration. In particular, the very low efficiencies of some PWNe could be associated with nearly aligned spin and magnetic axes. To check these hypotheses, it would be useful to look for a correlation between the PWN properties and multiwavelength pulsations.

1.2.9 General overview of the X-ray PWNe created by supersonically moving pulsars

About 15 X-ray PWNe created by pulsars moving through the ISM have been detected. The spindown powers $\dot{E}$ of these pulsars are in the range from 1.2×10^{33} erg s^{-1} (PSR B2224+65, the Guitar PWN) to 2.5×10^{36} erg s^{-1} (PSR J1747–2958, the Mouse PWN).
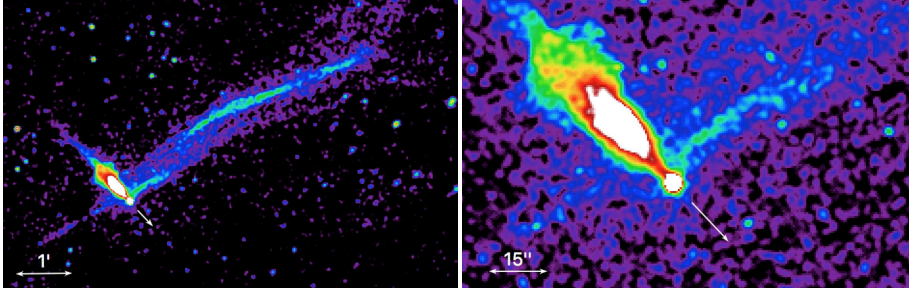
Fig. 15 *Chandra* ACIS image of the Lighthouse PWN (0.5–8 keV, 300 ks) created by PSR J1101–6101 ($\dot{E} = 1.4 \times 10^{36}$ erg s^{-1}, $\tau_{sd} = 116$ kyr) moving from the SNR MSH 11–61A (Pavan et al. 2016). The image shows a bright tail behind the fast-moving pulsar ($V_\perp \sim 1000 d_7$ km s^{-1}) and an $11 d_7$ pc long jet-like feature, possibly another example of a "misaligned outflow".

Electrons/positrons of PWs of less powerful pulsars, which consitute the majority of rotation-powered pulsars, apparently cannot be accelerated to energies high enough to emit X-ray synchrotron radiation, and even if the energy is sufficient, the PWN luminosity may be too low to detect it, even from nearby sources.

The presented examples show that most supersonically moving pulsars are accompanied by tails, with typical lengths of a few parsecs. However, the appearance of PWN heads vary considerably in different sources. Some of the well-resolved PWNe have a filled PWN head morphology (e.g., the Mouse, B0355+54, J1741–2044) while others show "hollow" morphologies (Geminga, J1509–5850). Moreover, there is at least one example, J0357+3205, which shows a long tail but no resolved PWN head around the pulsar. The diversity of PWN heads suggests that PWs of old pulsars are anisotropic, perhaps concentrated around the equatorial plane (like in the Crab and some other young pulsars) in many cases. The different appearances of the compact PWN components could be due to different orientations of the pulsar's spin axis with respect to the velocity direction and the line of sight. A particularly puzzling morphology is seen in the Geminga PWN, with its three "tails", which can be considered as a hollow-morphology compact PWN component observed from a close distance (it might have a much longer tail that is perhaps too faint to be detected by the current instruments).

Quite unexpected was the discovery of "misaligned outflows" in X-ray observations of several pulsars: B2224+65 (the Guitar), J1509–5850, B0355+54, described above, and likely the spectacular Lighthouse nebula created by PSR J1101–6101 (Pavan et al. 2016 and references therein; see Figure 1.2.9). Their nature still remains puzzling. A hypotheis was suggested by Bandiera (2008) that these features are produced by synchrotron radiation of very high energy particles leaked from the TSs into the ambient ISM along the ISM magnetic field, but this interpretation remains to be confirmed by a quantitative modeling.

Although the flow speeds along the tails or misaligned outflows have not been directly measured, they have been crudely estimated for some tails based on circumstantial arguments. These estimates show that flow speeds considerably exceed the pulsar speeds, but they are well below the mildly relativistic speeds predicted by the numerical simulations.

The X-ray efficiencies, $\eta_X = L_X/\dot{E}$, of the observed PWNe vary between $\lesssim 2 \times 10^{-6}$ (the alleged PWN around PSR B0656+14) and $\sim 10^{-2}$ (the Mouse). The reason for such a huge scatter remains unclear. At least partly, it can be due to different orientations of the pulsar equatorial planes, where the PWs are presumably concentrated, with respect to the pulsar velocities. It also may be that the fraction ξ_w of the spindown power lost to the PW is

different in different pulsars (because the fraction of $\dot{E}$ radiated from pulsar magnetospheres depends on pulsar parameters). Another likely reason for different PWN efficiencies is associated with conversion of the magnetic PW energy into the kinetic energy of particles, which should increase with increasing the angle between the magnetic and spin axes.

The X-ray spectra of PWNe created by supersonically moving pulsars are usually well described by a PL model, which supports their synchrotron interpretation. Typical spectral slopes Γ in the compact nebula components (PWN heads) are in the range of 1.5–2.0, but the lateral tails of the Geminga PWN are much harder, $\Gamma \sim 0.7$–1.0. Some of the PWN tails (e.g., in the Mouse and Lighthouse) show a substantial softening with increasing distance from the pulsar, up to $\Delta\Gamma \approx 1.0$–1.5, while others show no softening at all, sometimes even a hint of hardening. The fast softening is an indication of a relatively high magneting field (e.g., up to a few hundreds μG in the Mouse, the highest value found so far, which is a factor of 10 higher than typical magnetic fields).

A few head-tail PWNe have been detected in the radio. The radio tails are usually longer than the X-ray ones, as expected from the synchrotron cooling. The additional radio data allow one to examine a broad-band PWN spectrum, which is usually harder in the radio than in the X-rays, and get an idea about the spectrum of emitting particles. Measuring the spatially resolved radio polarization makes it possible to map the directions of the magnetic field within the PWN, but the two PWNe for which such mapping was done (the Mouse and J1509–5850) show very different distributions.

The X-ray spectral slopes $\Gamma < 2$ suggest that the main contribution to the total synchrotron PWN luminosities are provided by photons with energies above the observed X-ray range, i.e., above ~ 10 keV. However, none of the head-tail PWNe has been detected at hard X-rays or γ-rays, perhaps because the current detectors are not sensitive enough.

1.3 Open questions

Although many of the observed properties of PWNe produced by supesonically moving pulsars are qualitatively understood, there remain several problems that require further investigations, both observational and theoretical.

First of all, we should understand the reason(s) for the *great diversity of PWN shapes*. Although elongated X-ray tails behind the moving pulsars have been observed in many of them, it is not quite clear which parameters determine the tail properties (shape, length, collimation and divergence, separation from the pulsar in some cases). Even less clear is the origin of the divesity of PWN heads (e.g., filled vs. hollow morphology). One of such parameters is obviously the angle between the velocity vector and the line of sight, but other parameters, such as the angle between the spin and magnetic axes, and between the spin axis and the pulsar velocity, can play an important role. It is also possible that the direction and strength of the ambient ISM magnetic field can affect the observed surface brightness distribution. To assess the contribution of the different factors, a study of correlation of the PWN shape with the shapes and phases of pulsar pulses at different wavelengths (e.g., radio and γ-rays), supplemented by PWN modeling in the case of anisotropic PW, would be particularly useful.

The most puzzling features among the recently discovered PWN components are the "*misaligned outflows*", whose directions are strongly misaligned with respect to the pulsar velocities. It is tempting to interpret them as jets along the pulsar spin axes, similar to those observed in PWNe of young pulsars, but such jets are expected to be bent by the ram pressure on much smaller scales than the observed lengths of these nearly straight, elongated features.

Only qualitative interpretations of such features have been suggested so far, which remain to be confirmed by quantitative modeling.

It remains unclear whether "ordinary" *jets along the spin axes* have been detected in old PWNe outside SNRs. May it be that the outflows along the spin axis are less powerful (at least, less luminous) in old pulsars than in young ones? To answer this question, we should obtain independent information on the spin axis directions, which could be done with the aid of multiwavelength polarimetry, in addition to the pulse analysis.

Since the X-ray PWN emission is the synchrotron radiation from relativistic electrons and/or positrons, one should expect softening of the PWN spectrum with increasing distance from the pulsar due to synchrotron cooling. Such a softening has indeed been observed in some of the tails, but other tails, as well as the misaligned outflows, show *no spectral softening* at all, rather hints of hardening were observed. What is the reason for such behavior? Is it an indication of an additional (re)acceleration (heating) along the tails? What is the acceleration mechanism? Is it the same mechanism that is responsible for the unusually hard spectra of the Geminga's lateral tail? Why does it operate only in some tails? To answer these questions, deep high-resolution X-ray observations are required, which would allow spatially resolved spectral analysis to accurately measure the spectral changes. If the lack of softening (or even spectral hardening) is confirmed, possible acceleration mechanisms (e.g., the Fermi acceleration at fronts of oblique shocks or magnetic turbulence) should be studied.

Another puzzling problem is the *very low X-ray efficiency (or even the absence) of PWNe around some nearby pulsars* that are powerful enough to create an observable X-ray PWN. While it might be partly expained by closeness of the pulsar velocity direction to the line of sight, it is certainly not a full explanation. Are these PWNe so faint because the conversion of the PW magnetic energy into the particle energy (e.g., via magnetic field reconnection in the striped wind zone) is inefficient, as expected for pulsars with nearly aligned magnetic and spin axes? Are there other mechanisms that suppress the production and acceleration of the particle component of PWs? To understand the true reason, more nearby pulsars should be observed, and the absence or presence of PWNe should be confronted with the pulsar properties.

To conclude, a significant progress in our understanding of PWNe of supersonically moving pulsars has been achieved, thanks to the high resolution and sensitivity of the *Chandra* and *XMM-Newton* observatories, but there remain some open problems that could be resolved with further deep X-ray observations and more realistic modeling.

References

Z. Arzoumanian, D.F. Chernoff, J.M. Cordes, The Velocity Distribution of Isolated Radio Pulsars. Astrophys. J. **568**, 289–301 (2002). doi:10.1086/338805

K. Auchettl, P. Slane, R.W. Romani, B. Posselt, G.G. Pavlov, O. Kargaltsev, C.-Y. Ng, T. Temim, M.C. Weisskopf, A. Bykov, D.A. Swartz, X-Ray Analysis of the Proper Motion and Pulsar Wind Nebula for PSR J1741-2054. Astrophys. J. **802**, 68 (2015). doi:10.1088/0004-637X/802/1/68

R. Bandiera, On the X-ray feature associated with the Guitar nebula. Astron. Astrophys. **490**, 3–6 (2008). doi:10.1051/0004-6361:200810666

L. Bîrzan, G.G. Pavlov, O. Kargaltsev, Chandra Observations of the Elusive Pulsar Wind Nebula around PSR B0656+14. Astrophys. J. **817**, 129 (2016). doi:10.3847/0004-637X/817/2/129

N. Bucciantini, E. Amato, L. Del Zanna, Relativistic MHD simulations of pulsar bow-shock nebulae. Astron. Astrophys. **434**, 189–199 (2005). doi:10.1051/0004-6361:20042205

A. Bykov, N. Gehrels, H. Krawczynski, M. Lemoine, G. Pelletier, M. Pohl, Particle Acceleration in Relativistic Outflows. Space Sci. Rev. **173**, 309–339 (2012). doi:10.1007/s11214-012-9896-y

F. Camilo, R.N. Manchester, B.M. Gaensler, D.R. Lorimer, Heartbeat of the Mouse: A Young Radio Pulsar Associated with the Axisymmetric Nebula G359.23-0.82. Astrophys. J. Lett. **579**, 25–28 (2002). doi:10.1086/344832

P.A. Caraveo, G.F. Bignami, A. De Luca, S. Mereghetti, A. Pellizzoni, R. Mignani, A. Tur, W. Becker, Geminga's Tails: A Pulsar Bow Shock Probing the Interstellar Medium. Science **301**, 1345–1348 (2003). doi:10.1126/science.1086973

S. Chatterjee, J.M. Cordes, Bow Shocks from Neutron Stars: Scaling Laws and Hubble Space Telescope Observations of the Guitar Nebula. Astrophys. J. **575**, 407–418 (2002). doi:10.1086/341139

J.M. Cordes, R.W. Romani, S.C. Lundgren, The Guitar nebula - a bow shock from a slow-spin, high-velocity neutron star. Nature **362**, 133–135 (1993). doi:10.1038/362133a0

A. De Luca, M. Marelli, R.P. Mignani, P.A. Caraveo, W. Hummel, S. Collins, A. Shearer, P.M. Saz Parkinson, A. Belfiore, G.F. Bignami, Discovery of a Faint X-Ray Counterpart and a Parsec-long X-Ray Tail for the Middle-aged, γ-Ray-only Pulsar PSR J0357+3205. Astrophys. J. **733**, 104 (2011). doi:10.1088/0004-637X/733/2/104

A. De Luca, R.P. Mignani, M. Marelli, D. Salvetti, N. Sartore, A. Belfiore, P. Saz Parkinson, P.A. Caraveo, G.F. Bignami, PSR J0357+3205: A Fast-moving Pulsar with a Very Unusual X-Ray Trail. Astrophys. J. Lett. **765**, 19 (2013). doi:10.1088/2041-8205/765/1/L19

T. Dolch, S. Chatterjee, D.P. Clemens, J.M. Cordes, L.R. Cashmen, B.W. Taylor, Recent H-alpha Results on Pulsar B2224+65's Bow-Shock Nebula, the "Guitar". Journal of Astronomy and Space Sciences **33**, 167–172 (2016). doi:10.5140/JASS.2016.33.3.167

J. Faherty, F.M. Walter, J. Anderson, The trigonometric parallax of the neutron star Geminga. Astrophys. Space Sci. **308**, 225–230 (2007). doi:10.1007/s10509-007-9368-0

B.M. Gaensler, P.O. Slane, The Evolution and Structure of Pulsar Wind Nebulae. Ann. Rev. Astron. Astrophys. **44**, 17–47 (2006). doi:10.1146/annurev.astro.44.051905.092528

B.M. Gaensler, E. van der Swaluw, F. Camilo, V.M. Kaspi, F.K. Baganoff, F. Yusef-Zadeh, R.N. Manchester, The Mouse that Soared: High-Resolution X-Ray Imaging of the Pulsar-powered Bow Shock G359.23-0.82. Astrophys. J. **616**, 383–402 (2004). doi:10.1086/424906

C.A. Hales, B.M. Gaensler, S. Chatterjee, E. van der Swaluw, F. Camilo, A Proper Motion for the Pulsar Wind Nebula G359.23-0.82, the "Mouse," Associated with the Energetic Radio Pulsar J1747-2958. Astrophys. J. **706**, 1316–1322 (2009). doi:10.1088/0004-637X/706/2/1316

C.Y. Hui, W. Becker, X-ray emission properties of the old pulsar PSR B2224+65. Astron. Astrophys. **467**, 1209–1214 (2007). doi:10.1051/0004-6361:20066562

S.P. Johnson, Q.D. Wang, The pulsar B2224+65 and its jets: a two epoch X-ray analysis. Mon. Not. Royal Astron. Soc. **408**, 1216–1224 (2010). doi:10.1111/j.1365-2966.2010.17200.x

O. Kargaltsev, G.G. Pavlov, Pulsar Wind Nebulae in the Chandra Era, in *40 Years of Pulsars: Millisecond Pulsars, Magnetars and More*, ed. by C. Bassa, Z. Wang, A. Cumming, V.M. Kaspi American Institute of Physics Conference Series, vol. 983, 2008, pp. 171–185. doi:10.1063/1.2900138

O. Kargaltsev, B. Rangelov, G.G. Pavlov, Gamma-ray and X-ray Properties of Pulsar Wind Nebulae and Unidentified Galactic TeV Sources. ArXiv e-prints (2013)

O. Kargaltsev, Z. Misanovic, G.G. Pavlov, J.A. Wong, G.P. Garmire, X-Ray Observations of Parsec-scale Tails behind Two Middle-Aged Pulsars. Astrophys. J. **684**, 542–557 (2008). doi:10.1086/589145

C.F. Kennel, F.V. Coroniti, Confinement of the Crab pulsar's wind by its supernova remnant. Astrophys. J. **283**, 694–709 (1984). doi:10.1086/162356

J.G. Kirk, Y. Lyubarsky, J. Petri, The Theory of Pulsar Winds and Nebulae, in *Astrophysics and Space Science Library*, ed. by W. Becker Astrophysics and Space Science Library, vol. 357, 2009, p. 421. doi:10.1007/978-3-540-76965-1_16

N. Klingler, O. Kargaltsev, B. Rangelov, G.G. Pavlov, B. Posselt, C.-Y. Ng, Chandra Observations of Outflows from PSR J1509-5850. Astrophys. J. **828**, 70 (2016a). doi:10.3847/0004-637X/828/2/70

N. Klingler, B. Rangelov, O. Kargaltsev, G.G. Pavlov, R.W. Romani, B. Posselt, P. Slane, T. Temim, C.-Y.

Ng, N. Bucciantini, A. Bykov, D.A. Swartz, R. Buehler, Deep Chandra Observations of the Pulsar Wind Nebula Created by PSR B0355+54. Astrophys. J. **833**, 253 (2016b). doi:10.3847/1538-4357/833/2/253

M. Marelli, A. De Luca, D. Salvetti, N. Sartore, A. Sartori, P. Caraveo, F. Pizzolato, P.M. Saz Parkinson, A. Belfiore, PSR J0357+3205: The Tail of the Turtle. Astrophys. J. **765**, 36 (2013). doi:10.1088/0004-637X/765/1/36

K.E. McGowan, W.T. Vestrand, J.A. Kennea, S. Zane, M. Cropper, F.A. Córdova, Probing the Pulsar Wind Nebula of PSR B0355+54. Astrophys. J. **647**, 1300–1308 (2006). doi:10.1086/505522

R.P. Mignani, G.G. Pavlov, O. Kargaltsev, Optical-Ultraviolet Spectrum and Proper Motion of the Middle-aged Pulsar B1055-52. Astrophys. J. **720**, 1635–1643 (2010). doi:10.1088/0004-637X/720/2/1635

G. Morlino, M. Lyutikov, M. Vorster, Mass loading of bow shock pulsar wind nebulae. Mon. Not. Royal Astron. Soc. **454**, 3886–3901 (2015). doi:10.1093/mnras/stv2189

C.-Y. Ng, B.M. Gaensler, S. Chatterjee, S. Johnston, Radio Polarization Observations of G319.9-0.7: A Bow-Shock Nebula with an Azimuthal Magnetic Field Powered by Pulsar J1509-5850. Astrophys. J. **712**, 596–603 (2010). doi:10.1088/0004-637X/712/1/596

L. Pavan, G. Pühlhofer, P. Bordas, M. Audard, M. Balbo, E. Bozzo, D. Eckert, C. Ferrigno, M.D. Filipović, M. Verdugo, R. Walter, Closer view of the IGR J11014-6103 outflows. Astron. Astrophys. **591**, 91 (2016). doi:10.1051/0004-6361/201527703

G.G. Pavlov, S. Bhattacharyya, V.E. Zavlin, New X-ray Observations of the Geminga Pulsar Wind Nebula. Astrophys. J. **715**, 66–77 (2010). doi:10.1088/0004-637X/715/1/66

G.G. Pavlov, D. Sanwal, V.E. Zavlin, The Pulsar Wind Nebula of the Geminga Pulsar. Astrophys. J. **643**, 1146–1150 (2006). doi:10.1086/503250

B. Posselt, G. Spence, G.G. Pavlov, A Chandra Search for a Pulsar Wind Nebula around PSR B1055-52. Astrophys. J. **811**, 96 (2015). doi:10.1088/0004-637X/811/2/96

B. Posselt, G.G. Pavlov, P.O. Slane, R. Romani, N. Bucciantini, A.M. Bykov, O. Kargaltsev, M.C. Weisskopf, C.-Y. Ng, Geminga's puzzling pulsar wind nebula. ArXiv e-prints (2016)

R.W. Romani, M.S. Shaw, F. Camilo, G. Cotter, G.R. Sivakoff, The Balmer-dominated Bow Shock and Wind Nebula Structure of γ-ray Pulsar PSR J1741-2054. Astrophys. J. **724**, 908–914 (2010). doi:10.1088/0004-637X/724/2/908

M.M. Romanova, G.A. Chulsky, R.V.E. Lovelace, Winds, B-Fields, and Magnetotails of Pulsars. Astrophys. J. **630**, 1020–1028 (2005). doi:10.1086/431727

E. van der Swaluw, T.P. Downes, R. Keegan, An evolutionary model for pulsar-driven supernova remnants. A hydrodynamical model. Astron. Astrophys. **420**, 937–944 (2004). doi:10.1051/0004-6361:20035700

M. Vigelius, A. Melatos, S. Chatterjee, B.M. Gaensler, P. Ghavamian, Three-dimensional hydrodynamic simulations of asymmetric pulsar wind bow shocks. Mon. Not. Royal Astron. Soc. **374**, 793–808 (2007). doi:10.1111/j.1365-2966.2006.11193.x

M.C. Weisskopf, J.J. Hester, A.F. Tennant, R.F. Elsner, N.S. Schulz, H.L. Marshall, M. Karovska, J.S. Nichols, D.A. Swartz, J.J. Kolodziejczak, S.L. O'Dell, Discovery of Spatial and Spectral Structure in the X-Ray Emission from the Crab Nebula. Astrophys. J. Lett. **536**, 81–84 (2000). doi:10.1086/312733

F.P. Wilkin, Modeling Nonaxisymmetric Bow Shocks: Solution Method and Exact Analytic Solutions. Astrophys. J. **532**, 400–414 (2000). doi:10.1086/308576

D.S. Wong, J.M. Cordes, S. Chatterjee, E.G. Zweibel, J.P. Finley, R.W. Romani, M.P. Ulmer, Chandra Observations of the Guitar Nebula, in *High Energy Processes and Phenomena in Astrophysics*, ed. by X.D. Li, V. Trimble, Z.R. Wang IAU Symposium, vol. 214, 2003, p. 135

F. Yusef-Zadeh, J. Bally, A non-thermal axially symmetric radio wake towards the Galactic centre. Nature **330**, 455–458 (1987). doi:10.1038/330455a0

F. Yusef-Zadeh, B.M. Gaensler, A radio study of the mouse, G359.23 - 0.82. Advances in Space Research **35**, 1129–1136 (2005). doi:10.1016/j.asr.2005.03.003